NATIONAL ADVISORY COMMITTEE FOR AERONAUTICS

TECHNICAL NOTE 3761

TURBULENT SHEAR SPECTRA AND LOCAL ISOTROPY IN THE LOW-SPEED BOUNDARY LAYER

By Virgil A. Sandborn and Willis H. Braun

Lewis Flight Propulsion Laboratory
Cleveland, Ohio

Washington
September 1956

NATIONAL ADVISORY COMMITTEE FOR AERONAUTI...

TECHNICAL NOTE 3761

TURBULENT SHEAR SPECTRA AND LOCAL ISOTROPY IN THE LOW-SPEED BOUNDARY LAYER

By Virgil A. Sandborn and Willis H. Braun

SUMMARY

From measurements of turbulent shear spectra together with previously reported longitudinal turbulent energy spectra, the concept of local isotropy in a low-speed boundary layer was examined. Results of these measurements and measurements of the time derivatives of turbulent velocities in the x- and y-directions for various frequency bands showed no evidence of local isotropy in the boundary layer. Several methods (based on isotropy) of evaluating the turbulent dissipation term failed to give consistent answers, further emphasizing a lack of local isotropy.

INTRODUCTION

The most rewarding treatment of turbulent motion to date has been the statistical analysis introduced by Taylor (ref. 1). The analysis was first restricted to isotropic turbulence, in which there is no shear stress. In 1941, Kolmogoroff (refs. 2 and 3) hypothesized that the small-scale motions in high Reynolds number shear flows also possess the property of isotropy. This report examines evidence for the validity of Kolmogoroff's hypothesis in one type of shear flow, the turbulent boundary layer.

Previous tests of Kolmogoroff's theory of "local isotropy" have been made in turbulent wakes and jets, in turbulent channel flow, and to some extent in boundary layers. The first of these were the measurements made in the wake of a circular cylinder by Townsend (ref. 4), who found that several of the statistical quantities describing the flow agree with predictions of the theory. Corrsin and Uberoi (ref. 5) measured the cross correlation of the turbulent motion in a circular jet, and found that the correlation vanished for the small-scale motions, a possible sign of local isotropy. Laufer (refs. 6 and 7) also found that the cross correlation vanished in channel flow. However, his measurements of vorticity components, which give greater weight to the small-scale motions, do not indicate local isotropy.

The boundary layer, having one fixed edge and one free edge, is intermediate between channel and wake flow. Measurements made to detect local isotropy in the boundary layer have been inconclusive. Townsend (ref. 8) measured local vorticity componets in the boundary layer and compared them on the basis of complete isotropy. He found that the vorticity is not isotropic. This may have been due partly to contributions from the large-scale anisotropic motions and partly to the low Reynolds number of the flow. Klebanoff's (ref. 9) measurements of vorticity show an even more pronounced deviation from isotropy. He also obtained the over-all energy balance by integration across the boundary layer and concluded that the assumption of local isotropy was not adequate for the flow.

SYMBOLS

The following symbols are used in this report:

A	constant
d	half width of channel
$E(k)$	three-dimensional energy spectrum function associated with wave-number space
$F(n)$	one-dimensional energy spectrum function associated with frequency
$f(k)$	one-dimensional energy spectrum function associated with wave-number space
k	wave number
L_x	longitudinal turbulence scale $\int_0^\infty R_x \, dx$
n	frequency
p	static pressure at wall
R_{uv}	correlation coefficient of the turbulent velocities u and v at a particular point for all frequencies, $\frac{\overline{uv}}{\sqrt{\overline{u^2}}\sqrt{\overline{v^2}}}$
$R_{\overline{uv},n}$	correlation coefficient of the turbulent velocities u and v at a particular point and frequency n, $\frac{\overline{uv}_n}{\sqrt{\overline{u_n^2}}\sqrt{\overline{v_n^2}}}$

R_x	correlation coefficient of u in the x-direction
t	time
U	local mean velocity
U_0	mean velocity in free stream where viscous effects are unimportant
ν'	velocity parameter in universal equilibrium theory
u,v,w	instantaneous turbulent velocities in x-, y-, and z-directions, respectively
$\overline{u^2}$, $\overline{v^2}$, $\overline{w^2}$	mean squares of turbulent velocity fluctuations in x-, y-, and z-directions, respectively
$\overline{uv}$	Reynolds turbulent shear stress
x	direction parallel to test wall and in general direction of mean flow
y	direction normal to test wall and approximately normal to mean flow
z	direction normal to mean flow and parallel to test wall
δ	boundary-layer thickness
ε	turbulent energy dissipation per unit mass of fluid
η	length parameter in universal equilibrium theory
ν	kinematic viscosity

UNIVERSAL EQUILIBRIUM THEORY

Before a discussion of the present data is made, a brief review of pertinent results of the universal equilibrium theory is necessary. (For a full treatment of the subject, see ref. 10.)

Turbulence is pictured as a group of eddies of various sizes, the largest of which derive energy from the mean motion of the fluid. These large eddies are unstable and decay into smaller eddies. Kolmogoroff suggests that, for "sufficiently high" Reynolds numbers, the smaller eddies have a small period compared with that of the large eddies. The small eddies are therefore almost statistically steady during a period

of time characteristic of the large eddies or over-all flow. Furthermore, the small eddies are unaware of the anisotropy of the large eddies. The small eddies dissipate, by viscous action, nearly all the energy entering the motion through the large eddies. The statistical properties of the small eddies are then determined by only two numbers, the time rate of specific energy dissipation ε and the kinematic viscosity ν of the fluid. From these parameters, a basic length and velocity are defined as

$$\eta = \left(\frac{\nu^3}{\varepsilon}\right)^{1/4}$$

and

$$v = (\nu\varepsilon)^{1/4}$$

η and v are measures of the characteristic length and velocity of the smallest eddies. When lengths and velocities are referenced to these parameters, the motion can be expressed in universal form.

It is evident that the evaluation of ε is of particular interest. The general expression for ε is (ref. 1)

$$\varepsilon = \nu\left[2\overline{\left(\frac{\partial u}{\partial x}\right)^2} + 2\overline{\left(\frac{\partial v}{\partial y}\right)^2} + 2\overline{\left(\frac{\partial w}{\partial z}\right)^2} + \overline{\left(\frac{\partial v}{\partial x} + \frac{\partial u}{\partial y}\right)^2} + \overline{\left(\frac{\partial w}{\partial y} + \frac{\partial v}{\partial z}\right)^2} + \overline{\left(\frac{\partial u}{\partial z} + \frac{\partial w}{\partial x}\right)^2}\right] \tag{1}$$

The restriction to isotropic turbulence leads to the simple form (ref. 1)

$$\varepsilon = 15\nu\overline{\left(\frac{\partial u}{\partial x}\right)^2} \tag{2}$$

The energy spectrum may also be used to express ε in isotropic turbulence. From a Fourier transform of the Kármán-Howarth (ref. 11) equation, ε may be written as

$$\varepsilon = 2\nu\int_0^\infty k^2E(k)\,dk \tag{3}$$

where k is the wave number and $E(k)$ is the three-dimensional spectrum function. This spectrum function $E(k)$ is related to the

measurable one-dimensional spectrum function $f(k_1)$ for isotropic turbulence by the following relation given by Heisenberg (ref. 12):

$$E(k) = k^3 \frac{d}{dk}\left[\frac{1}{k}\frac{d}{dk} f(k)\right] \tag{4}$$

Thus, ε expressed in terms of the measured spectrum function $F(n)$ and frequency is (ref. 13).

$$\varepsilon = \frac{8\pi^2 \nu \overline{u^2}}{U^2} \int_0^\infty \left\{ n^2 F(n) + 4 \int_\infty^n nF(n)\, dn \right\} dn \tag{5}$$

The relation between wave number and frequency is

$$k = \frac{2\pi n}{U} \tag{6}$$

The theory of local isotropy makes certain predictions about the form of the spectrum $E(k)$ and thus $F(n)$. The first concerns the form of the spectrum in the inertial subrange of wave numbers. For this range, inertial forces predominate and the spectrum is independent of ν and has the form

$$E(k) \sim \varepsilon^{2/3} k^{-5/3} \tag{7}$$

If, along with the spectrum $F_{\overline{u^2}}(n)$ of the mean square of the longitudinal component $\overline{u^2}$, one also considers the spectrum of the shear stress $F_{\overline{uv}}(n)$ certain contrasts should appear. At high frequencies, if the theory of local isotropy applies, the spectrum $F_{\overline{uv}}(n)$ should vanish faster than the energy spectrum $F_{\overline{u^2}}(n)$.

To test for local isotropy in the boundary layer, measurements of the turbulent shear spectra will be examined. If local isotropy exists, it is expected that the turbulent shear stress will vanish at the high frequencies in agreement with the definition of isotropy. Secondly, the energy spectrum of the longitudinal turbulent velocity will be examined for the existence of an inertial subrange. And finally, a specific relation predicted by isotropy between the turbulent velocity derivatives will be examined experimentally. From the velocity derivatives, a range of eddy sizes can be inferred.

MEASUREMENTS

The data reported herein correspond to the flow described in reference 14. Figure 1 is a schematic diagram of the boundary-layer channel. Measurements were made at the most forward and most aft of four stations previously used. The flow conditions were maintained constant, so that a Reynolds number per foot of 2.9×10^5 (which was equivalent to a free-stream velocity of approximately 49 ft/sec) was maintained at station 1. A constant pressure drop of approximately 25 inches of water below atmospheric was maintained in each suction compartment of the porous wall. A gradual change in the porosity of the porous wall over the span of measurements caused some variation in flow conditions; however, this flow variation is small compared with the random error of any single turbulence measurement. The respective pressure gradients at the stations were 0.012 and 0.194 pound per square foot per foot.

Mean and Turbulent Velocities

The mean velocity and turbulent intensity distributions for test stations 1 and 4 are shown in figures 2 and 3. Details of technique and equipment used for the measurements are reported in reference 15. The mean velocity profiles are the same as reported in reference 14, but the longitudinal turbulent velocities are recent measurements. They agree with the values previously reported within approximately 10 percent. The data of reference 14 and this report were taken over a 2-year period; thus the 10-percent variation represents about the limit of flow repeatability. The turbulent intensity in the z-direction $\sqrt{\overline{w^2}}$ (not shown) agrees with the turbulent intensity in the y-direction $\sqrt{\overline{v^2}}$, with only a slight deviation near the wall. This has previously been noted in reference 15.

Turbulent Shear Stress and Spectra

Faired curves of the turbulent shear stress at stations 1 and 4 are shown in figure 4. The turbulent shear-stress spectral distributions are shown in figure 5. (The spectra of the longitudinal turbulent velocities corresponding to the same flow are reported in ref. 14.) For the high frequencies, the measured points are least accurate as they represent the difference of two nearly equal hot-wire signals. In certain cases, negative values of $F_{\overline{uv}}(n)$ were computed from the experimental data. While there is no reason to rule out negative values of $F_{\overline{uv}}(n)$, it was impossible to plot them on the logarithmic scale of figure 5. The solid curves of figure 5 were obtained by subtracting curves faired

through the data of individual hot wires. The fairings were such that no negative values resulted. The integral $\int_0^\infty F_{\overline{uv}}(n)\,dn$ equals unity within approximately ±20 percent for all the spectra.

Determination of Time Derivatives

Statistical mean square time derivatives of the turbulent velocities u and v were measured. An electronic differentiation circuit similar to the one described by Townsend (ref. 16) was used. A variable electronic filter was employed to determine the contribution to the time derivatives from different frequency bands. With the filter set to cut out frequencies below a particular value of n, only the contributions from the higher frequencies were recorded. It was expected that by varying the cutoff frequency, a minimum frequency associated with the region of local isotropy might be found. The degree to which this expectation is met will be discussed later.

The high-frequency measurements proved difficult, as the measuring system was sensitive to any noise occurring in the area surrounding the tunnel. In particular, the differentiating circuit amplified the high-frequency noise. However, it is believed that careful observation reduced error from this source to a small random amount. It is estimated that the internal noise of the electronic system could have contributed no more than a 10-percent error even at the highest frequencies. An estimate of the accuracy of the time-derivative spectrum measurements was not made.

DISCUSSION

Spectral Distribution

Figure 6 shows a comparison of $\overline{u^2}$, $\overline{v^2}$, and $\overline{uv}$ spectra near the wall at station 1. For the high frequencies, the percentage energy density does not differ greatly for the three spectra. For the lower frequencies, a dip is usually noted in the $\overline{v^2}$ spectrum. Measurements of the $\overline{w^2}$ spectrum (not shown) are very nearly the same as the $\overline{v^2}$ spectrum with the possible exception of the dip at low frequencies. No particular effect of pressure gradient was observed (this observation corresponds to the trends of measurements for $\overline{u^2}$ in ref. 14).

The assumption of local isotropy leads to a variation of F(n) as $n^{-5/3}$ (eq. (7)) for an inertial subrange of frequencies. In figure 7,

a line with slope of -5/3 has been fitted to the $\overline{u^2}$ data. The line of -5/3 slope approximates a region for each of the spectra. But the nature of the spectral curves is such that any value of slope between zero and roughly -7 would be reasonable at some frequency. Thus, it is doubtful whether the fit of a line of -5/3 slope can be regarded as a check of the assumption of an inertial subrange.

Comparison of Second Moments of Spectra

Any difference in behavior between the $F_{\overline{uv}}(n)$ and $F_{\overline{u^2}}(n)$ spectra at high frequencies can be more readily observed by comparing their second moments. These second moments are only a device for examining the high-frequency portion of the spectra. Although the second moment of the three-dimensional energy spectrum of isotropic turbulence represents the viscous dissipation at any frequency in terms of the one-dimensional energy spectrum, the dissipation must be expressed by a sum of the first and second moments, as given by equation (5). Consequently, the second moments of the one-dimensional spectra presented here do not have a physical meaning. Laufer (ref. 6) has compared the second moments of the spectral distributions of $\overline{u^2}$ and $\overline{uv}$ at a particular y-distance in a two-dimensional channel (fig. 8). He notes that, at frequencies over 1500 cycles per second, essentially no correlation exists between u and v; thus indicating that local isotropy may occur.

This condition of vanishing correlation between u and v is necessary for local isotropy to exist, but it is not a sufficient condition. Since Laufer finds a very clear-cut region in which isotropy may exist, it appears worthwhile to apply the same tests to the boundary-layer data. Figure 9 shows the comparison between the second moments of the $\overline{uv}$ and $\overline{u^2}$ spectra for the measurements of this report. Inserted on figure 9 are the dimensional second moments $n^2\,\overline{u^2}\,F_{\overline{u^2}}(n)$ and $-n^2\,\overline{uv}\,F_{\overline{uv}}(n)$. The $\overline{v^2}$ moment at certain y-distances is also included on the dimensional plots.

The dimensional curves give an idea of the relative values of the three Reynolds stresses at any frequency. For local isotropy, the conditions $\overline{u_n^2} \cong \overline{v_n^2}$ and $\overline{uv}_n \to 0$ would be expected. For the present measurements, these conditions are not strongly evident. In the range where the -5/3 power law fits the spectra, it was found that

$$\overline{u_n^2} \cong \overline{v_n^2} > 2(\overline{uv})_n$$

This corresponds to a cross correlation coefficient $R_{\overline{uv},n} \cong 0.25$, which is still the same order of magnitude as the over-all value of $R_{\overline{uv}} \cong 0.5$. Thus, the shear stress in the high-frequency motions is relatively as strong as in the low-frequency motions. Corrsin and Uberoi (ref. 5) have pointed out that the approach to zero, at high frequencies, of the correlation coefficient spectrum is a necessary condition for local isotropy. Thus, it is concluded that there is no local isotropy in the boundary layer. This point is further illustrated in figure 10, which shows the distribution with frequency of the correlation coefficient $\left(R_{\overline{uv},n}/R_{\overline{uv}} \cong \frac{F_{\overline{uv}}(n)}{F_{\overline{u^2}}(n)\ F_{\overline{v^2}}(n)}\right)$ for two y-distances at station 4. These spectra are not examined in detail here, since they represent the same results shown in the second-moment curves.

It appears, then, that the boundary-layer flow investigated here, and the channel flow studied by Laufer in reference 6 have different properties. Although the Reynolds numbers based on boundary-layer thickness and channel width for the two flows were roughly the same (the former being slightly larger), evidence of local isotropy appears only in the channel flow.

The range of frequencies over which a line of $-5/3$ slope fits the $\overline{u^2}$ spectrum is very near the maximum of the second-moment curve. Although no physical meaning is as yet directly associated with the second-moment curve, it is suggested by the present measurements that for the boundary-layer flow the maximum roughly separates the frequency range of the large energy-containing eddies from the frequency range, wherein energy is dissipated by viscous forces.

Mean Square Velocity Derivatives

For isotropic turbulence it has been shown that (ref. 1)

$$\overline{\left(\frac{du}{dx}\right)^2} = \frac{1}{2}\overline{\left(\frac{dv}{dx}\right)^2} \tag{8}$$

If, the equivalence of space and time averages is assumed, equation (8) can be written as

$$\overline{\left(\frac{du}{dt}\right)^2} = \frac{1}{2}\overline{\left(\frac{dv}{dt}\right)^2} \tag{9}$$

The time derivatives can be obtained from hot-wire measurements. Townsend (ref. 4) has measured the derivatives in a turbulent wake and found them to agree with equation (9). From the agreement, he concluded that a strong basis for local isotropy existed. However, for the boundary layer, Townsend (ref. 8), as well as Klebanoff (ref. 9), found that the derivatives did not obey equation (9). The measurements themselves cannot indicate whether the disagreement was due to anisotropy at all wave numbers or whether contributions from the anisotropic small-wave-number region were overshadowing a high-frequency isotropic region. In the latter case, the existence of local isotropy is still possible.

The spectra of the derivatives were measured in order to discover the ranges of frequency over which the anisotropy exists. If there is local isotropy then as stated previously at higher frequencies $\overline{\left(\frac{du}{dt}\right)^2} = \frac{1}{2}\overline{\left(\frac{dv}{dt}\right)^2}$. An equivalent comparison of $3\overline{\left(\frac{du}{dt}\right)^2}$ and $\overline{\left(\frac{du}{dt}\right)^2} + \overline{\left(\frac{dv}{dt}\right)^2}$ for frequencies above the filter cutoff frequency n is made in figure 11. (The terms most readily measured with the hot wire are $3\overline{\left(\frac{du}{dt}\right)^2}$ and $\overline{\left(\frac{du}{dt}\right)^2} + \overline{\left(\frac{dv}{dt}\right)^2}$.) The accuracy of measurement at the high frequencies is low, as noted previously; however, the trends indicated by the data are quite consistent for the complete set.

In general, the spectra do not indicate local isotropy. At two points of station 1 (figs. 11(b) and (c)) the curves coincide for certain frequencies, but the second-moment curves (figs. 9(b) and (c)) show that the cross correlations are not small in the same range. The coincidence of these curves apparently has no significance. At the high frequencies almost all the curves tend to diverge.

Turbulent Energy Dissipation

It was previously noted that the assumptions of local isotropy greatly facilitate the calculation of the turbulent energy dissipation ε. While the present measurements do not justify the use of isotropic relations in the boundary layer, it is still of interest to determine the extent to which the isotropic predictions of ε are usable.

Four available methods of computing ε are

(1) Measurement of the terms of equation (1)

(2) Taylor's isotropic relation (eq. (2))

(3) Evaluation from the longitudinal spectrum measurement (eq. (5))

(4) Predictions of an inertial subrange (eq. (7)) from which $\varepsilon^{2/3}$ multiplied by a proportionality constant can be obtained

Klebanoff (ref. 9) used method (1) by writing ε as

$$\varepsilon = \nu \frac{d^2}{dy^2}\left(\frac{\overline{u^2} + \overline{v^2} + \overline{w^2}}{2}\right) - \nu\left[\overline{\left(\frac{\partial u}{\partial x}\right)^2} + \overline{\left(\frac{\partial v}{\partial x}\right)^2} + \overline{\left(\frac{\partial w}{\partial x}\right)^2} + \overline{\left(\frac{\partial u}{\partial y}\right)^2} + \overline{\left(\frac{\partial u}{\partial z}\right)^2} + \overline{\left(\frac{\partial v}{\partial y}\right)^2} + \overline{\left(\frac{\partial v}{\partial z}\right)^2} + \overline{\left(\frac{\partial w}{\partial y}\right)^2} + \overline{\left(\frac{\partial w}{\partial z}\right)^2}\right] \tag{1a}$$

$$\left(\frac{\partial^2}{\partial x^2} \text{ and } \frac{\partial^2}{\partial z^2} \text{ neglected}\right)$$

Of these terms, all but the last four derivatives were evaluated from hot-wire measurements. The last four terms were evaluated by using isotropic relations. Figure 12 shows the values of ε obtained by Klebanoff. Values of ε obtained from methods (2) and (3) for Klebanoff's data are also shown.

Klebanoff's evaluation of ε from equation (1a) is used as a standard for comparison with other methods. The use of Taylor's equation (eq. (2)) is found to predict a value too large for the dissipation for the outer region of the boundary layer, while near the wall it gives a value much too small. The value of ε obtained from the spectrum (method (3)) is too low over the complete boundary layer. This is partly due to the assumption of isotropy in Heisenberg's transformation from the three-dimensional spectrum to the one-dimensional spectrum. For Klebanoff's flow, the values of ε calculated by methods (2) and (3) bracket the correct value over most of the boundary layer; however, near the wall all isotropic evaluations are too low. The value of the proportionality constant A of equation (7) (now written in terms of the one-dimensional spectrum) which would scale up the curve of method (4) to the reference curve in the middle region of the boundary layer (from y/δ of 0.2 to 0.6), is between 0.30 and 0.35. For the outer region and near the wall, the constant varies sharply with y/δ.

Figure 13 presents the values of ε determined by methods (2), (3), and (4) for the data of this report measured at station 1. The approximately zero pressure gradient layer of station 1 shows the same general trends as Klebanoff's data, with the exception of the values near the wall. Hence, for the boundary layer examined here, the true value of the dissipation ε is expected to fall between curves of methods (2) and (3) in the outer region.

Values of the universal equilibrium parameters η and ν computed from ε and ν are plotted nondimensionally in figure 14. Over most of the boundary layer, $\eta\sqrt{\overline{u^2}}/\nu$ is equal approximately to 6, or η is of the order of 10^{-3} inches, approximately 1000 mean free paths of air at the test conditions. The value of η corresponds to a measuring frequency of the order of 10,000 cycles per second.

CONCLUDING REMARKS

Since, as a whole, the data presented here do not seem to describe a locally isotropic flow, some of the conditions prescribed by the theory are not met. Possible reasons why local isotropy was not found are as follows:

(1) The Reynolds number of the flow was too low.

(2) The physical picture which is hypothesized for turbulence is not adequate.

(3) Energy may be entering the spectra at high wave numbers.

It is difficult to construct a Reynolds number that characterizes the turbulence. Batchelor (refs. 3 and 10) has converted the criterion for local isotropy behind a grid from one involving Reynolds number to one depending on a scale ratio. It is necessary that the scale of the energy-containing eddies be very large compared with the scale of the small, stable eddies. If L_x is the macroscale of the turbulence, and η is again the characteristic diameter of the small eddies, then

$$\frac{L_x}{\eta} \gg 1$$

For the boundary layer data presented here,

$$\frac{L_x}{\eta} \sim 10^2 \sim 2^7$$

where L_x is the x-direction scale of $\overline{u^2}$. From the foregoing it is possible to estimate the number of steps occurring in the eddy cascade process. If eddies break up into other eddies one-tenth their size, there are only two ranges of size or orders of magnitude present, whereas if they break up into eddies one-half their size, there are about seven orders of magnitude present. It may be that there is not a sufficient spread in eddy size for the theory to apply to this shear flow.

Batchelor and Townsend (ref. 17) have pointed out that, in general, turbulence is not Gaussian at the high frequencies. This follows from their measurements which indicate an uneven distribution (in space) of the energy associated with the large wave-number region. It is impossible to estimate the effect of this "spottiness" on local isotropy, but it is certainly not the model assumed by the theory. The other suggested reason for the apparent absence of isotropy is that energy may be entering the spectrum at the high wave numbers. The measurements of Klebanoff (ref. 9) might suggest an excess production of turbulent energy in the high wave numbers, since near the wall the production and dissipation are not equal. Possibly small eddies, as well as large ones, are produced near the wall and diffuse outward into the boundary layer, thus masking isotropy in the cascades initiated by the large eddies.

Lewis Flight Propulsion Laboratory
National Advisory Committee for Aeronautics
Cleveland, Ohio, May 10, 1956

REFERENCES

1. Taylor, G. I.: Statistical Theory of Turbulence, pt. II. Proc. Roy. Soc. (London), ser. A, vol. 151, no. 833, 1935, pp. 444-454.

2. Kolmogoroff, A. N.: The Local Structure of Turbulence in Incompressible Viscous Fluid for Very Large Reynolds Numbers. Comp. Rend., vol. XXX, no. 4, 1941, pp. 301-305.

3. Batchelor, G. K.: Kolmogoroff's Theory of Local Isotropic Turbulence. Proc. Cambridge Phil. Soc., vol. 43, pt. 4, 1947, pp. 533-559.

4. Townsend, A. A.: Local Isotropy in the Turbulent Wake of a Cylinder. Australian Jour. Sci. Res., ser. A, vol. 1, no. 2, June 1948, pp. 161-174.

5. Corrsin, Stanley, and Uberoi, Mahinder S.: Spectra and Diffusion in a Round Turbulent Jet. NACA Rep. 1040, 1951. (Supersedes NACA TN 2124.)

6. Laufer, John: Some Recent Measurements in a Two-Dimensional Turbulent Channel. Jour. Aero. Sci., vol. 17, no. 5, May 1950, pp·277-287.

7. Laufer, John: Investigation of Turbulent Flow in a Two-Dimensional Channel. NACA Rep. 1053, 1951. (Supersedes NACA TN 2123.)

8. Townsend, A. A.: The Structure of the Turbulent Boundary Layer. Proc. Cambridge Phil. Soc., vol. 47, pt. 2, 1950, pp. 375-395.

9. Klebanoff, P. S.: Characteristics of Turbulence in a Boundary Layer with Zero Pressure Gradient. NACA TN 3178, 1954.

10. Batchelor, G. K.: The Theory of Homogeneous Turbulence. Cambridge Univ. Press, 1953.

11. von Kármán, Theodore, and Howarth, Leslie: On the Statistical Theory of Isotropic Turbulence. Proc. Roy. Soc. (London), ser. A, vol. 164, Jan. 21, 1938, pp. 192-215.

12. Heisenberg, W.: Zur statistischen Theorie der turbulenz. Zs. f. Phys., Bd. 124, Heft 7/12, 1948, pp. 628-657.

13. Lin, C. C.: Remarks on the Spectrum of Turbulence. Proc. Symposia of Appl. Math. Vol. 1. Am. Math. Soc., 1949, pp. 81-86.

14. Sandborn, Virgil A., and Slogar, Raymond J.: Longitudinal Turbulent Spectrum Survey of Boundary Layers in Adverse Pressure Gradients. NACA TN 3453, 1955.

15. Sandborn, Virgil A., and Slogar, Raymond J.: Study of the Momentum Distribution of Turbulent Boundary Layers in Adverse Pressure Gradients. NACA TN 3264, 1955.

16. Townsend, A. A.: The Measurement of Double and Triple Correlation Derivatives in Isotropic Turbulence. Proc. Cambridge Phil. Soc., vol. 43, pt. 4, Oct. 1947, pp. 560-570.

17. Batchelor, G. K., and Townsend, A. A.: The Nature of Turbulent Motion at Large Wave-Numbers. Proc. Roy. Soc. (London), ser. A, vol. 199, no. A 1057, Oct. 25, 1949, pp. 238-255.

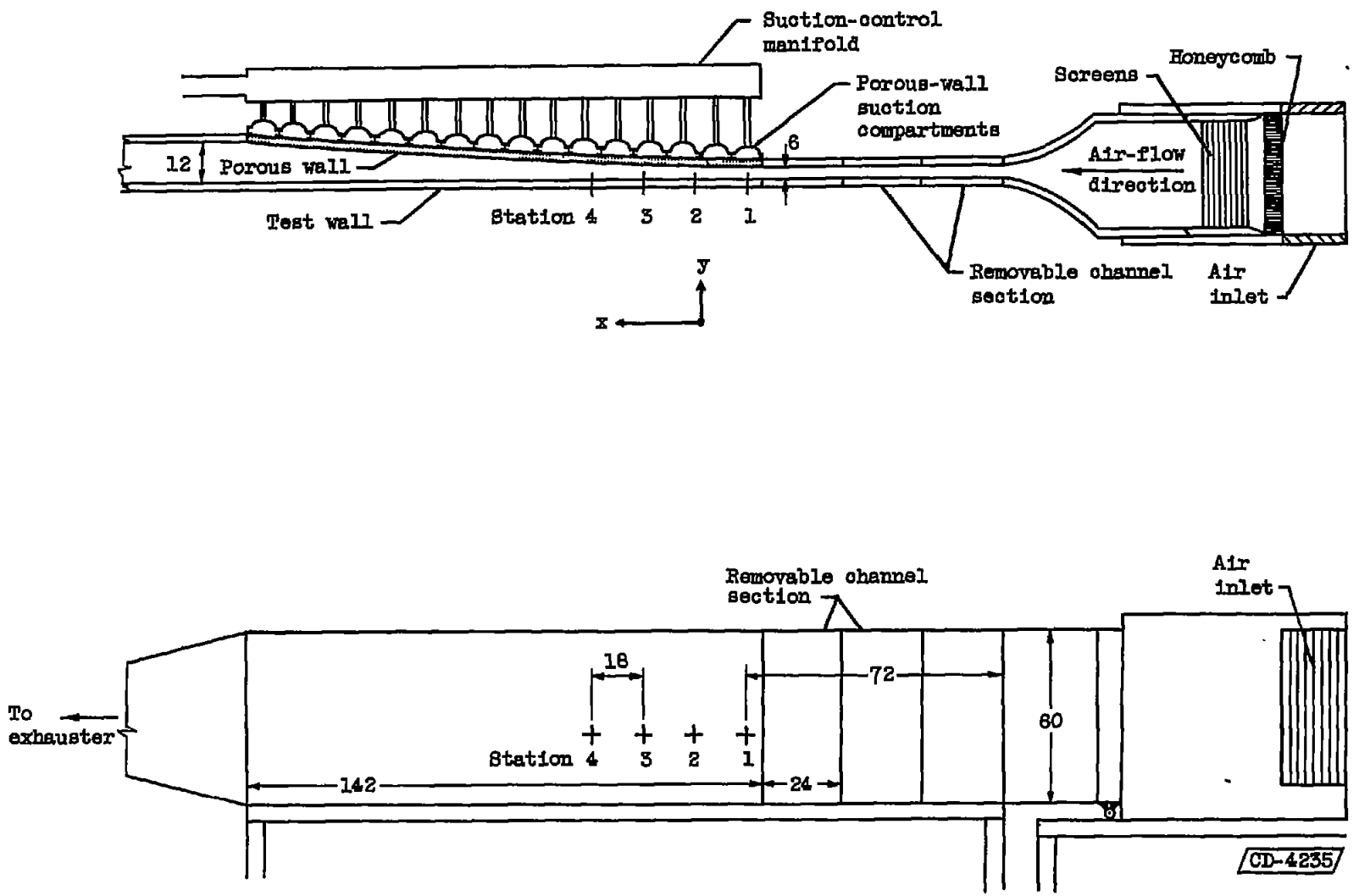

Figure 1. - Diagram of 6- by 60-inch subsonic boundary-layer channel. (All dimensions in inches.)

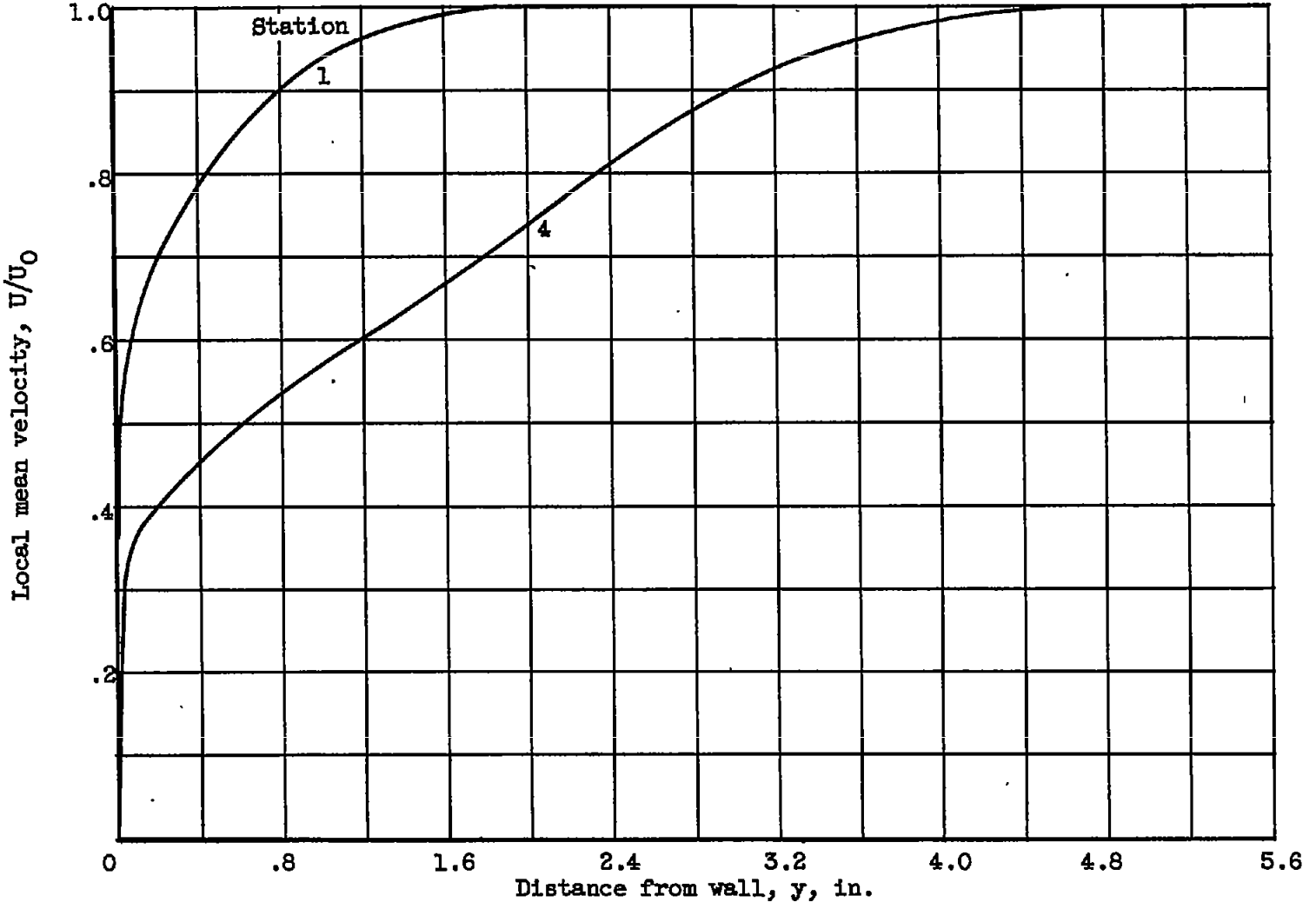

Figure 2. - Mean velocity distribution through boundary layer. Stations 1 and 4.

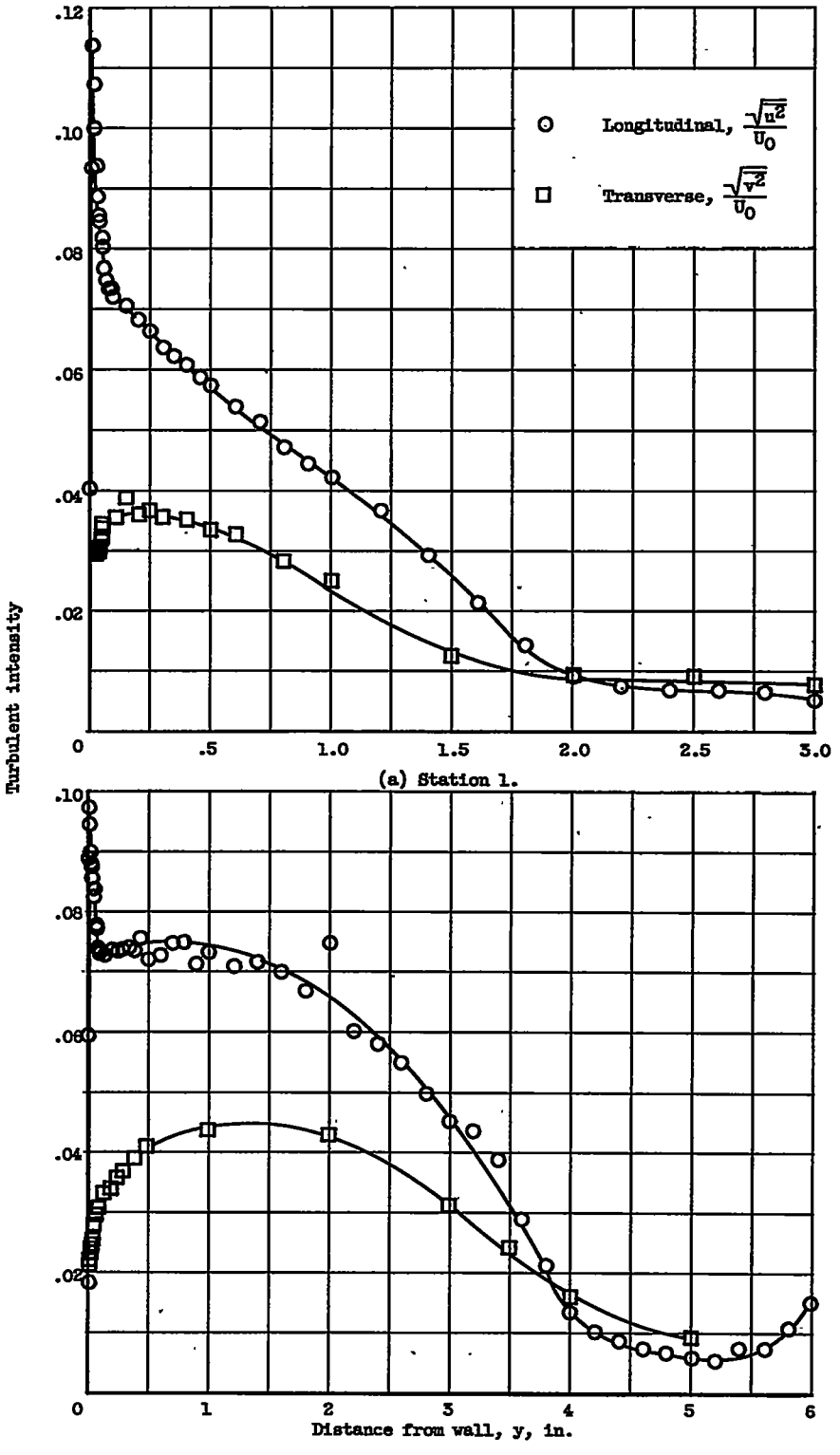

Figure 3. - Turbulent velocity distributions through boundary layer.

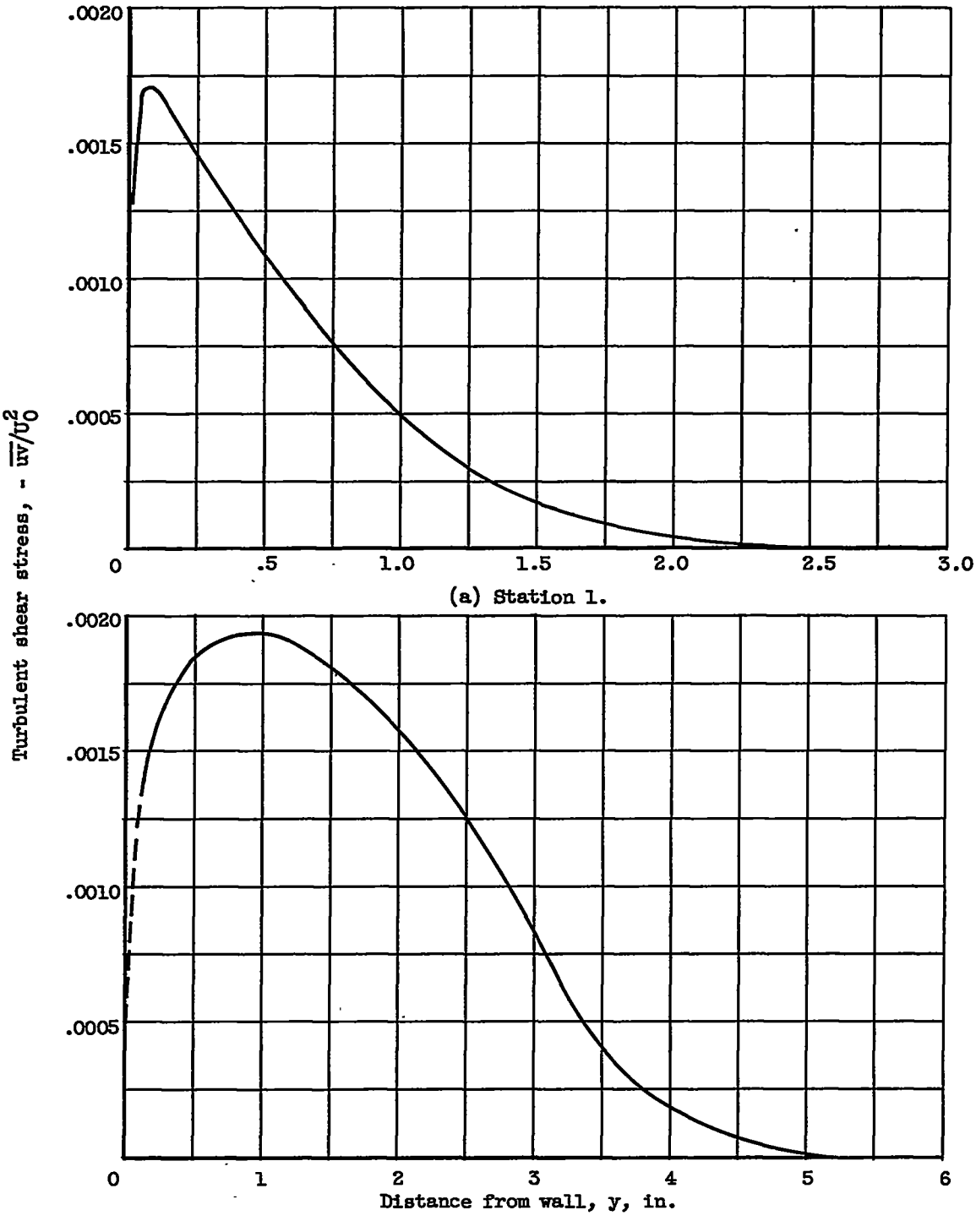

Figure 4. - Turbulent shear stress distribution through boundary layer.

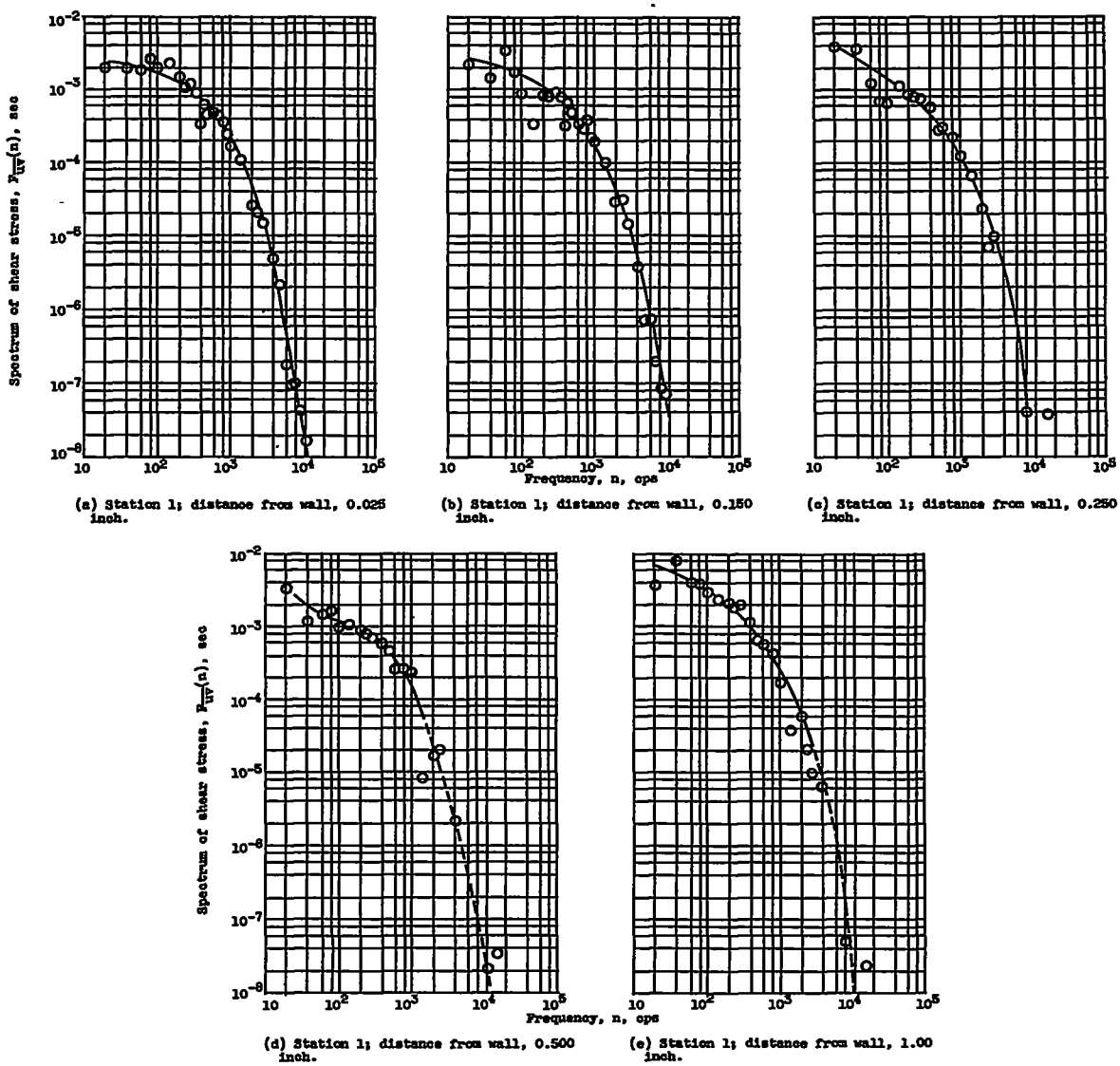

(a) Station 1; distance from wall, 0.025 inch.

(b) Station 1; distance from wall, 0.150 inch.

(c) Station 1; distance from wall, 0.250 inch.

(d) Station 1; distance from wall, 0.500 inch.

(e) Station 1; distance from wall, 1.00 inch.

Figure 5. - Turbulent shear stress spectrum.

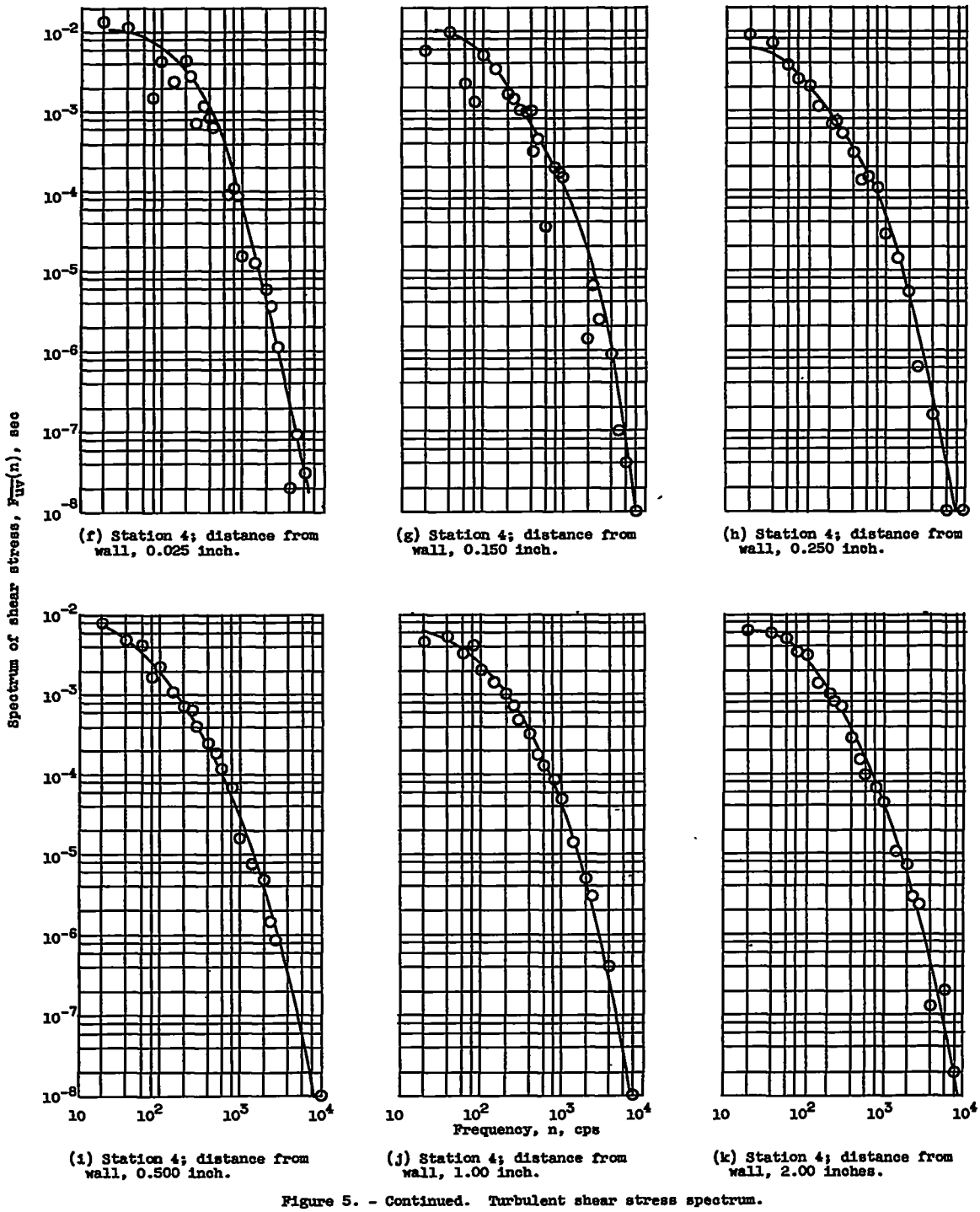

(f) Station 4; distance from wall, 0.025 inch.

(g) Station 4; distance from wall, 0.150 inch.

(h) Station 4; distance from wall, 0.250 inch.

(i) Station 4; distance from wall, 0.500 inch.

(j) Station 4; distance from wall, 1.00 inch.

(k) Station 4; distance from wall, 2.00 inches.

Figure 5. - Continued. Turbulent shear stress spectrum.

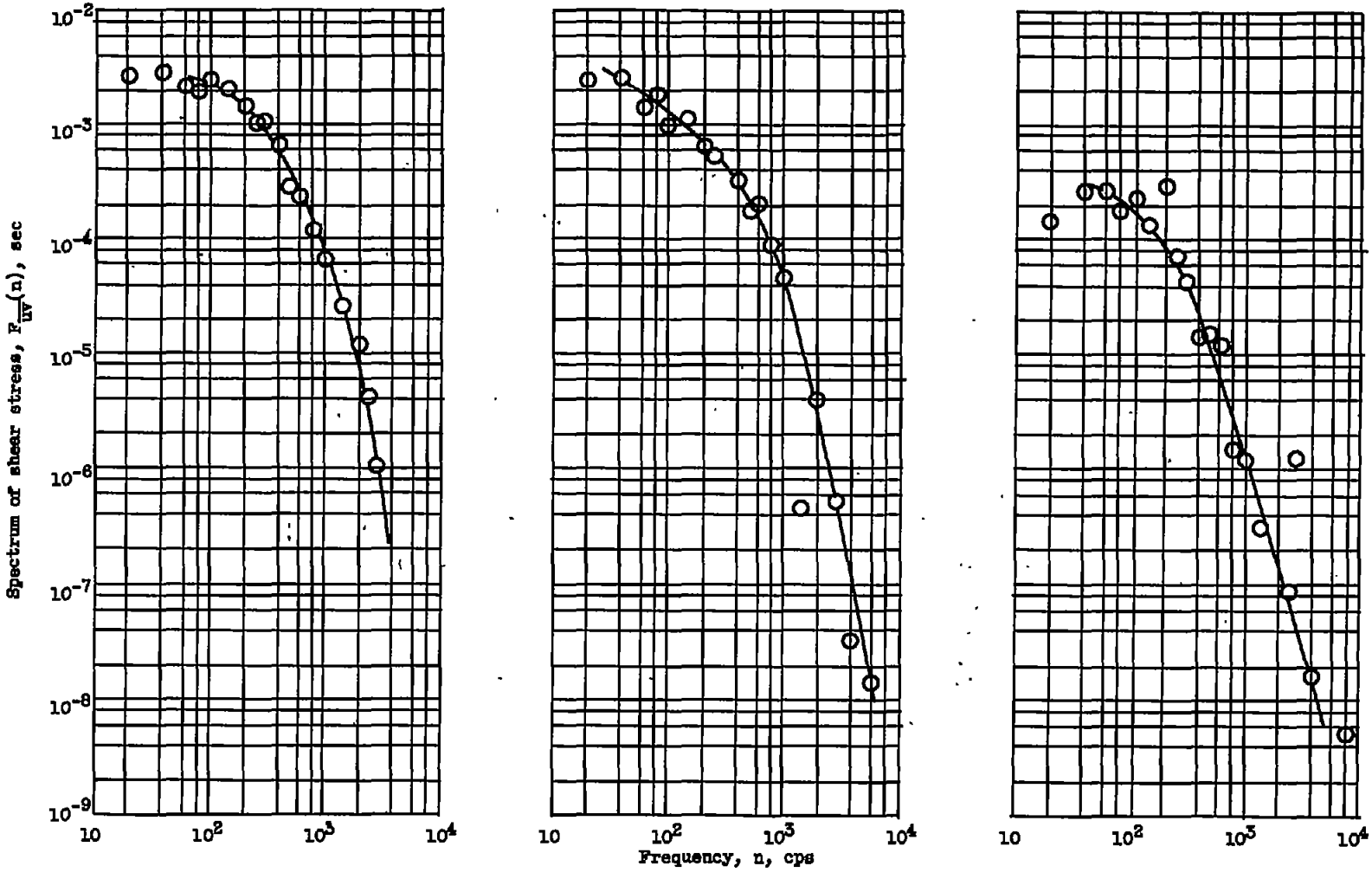

(l) Station 4; distance from wall, 3.00 inches.

(m) Station 4; distance from wall, 3.50 inches.

(n) Station 4; distance from wall, 4.00 inches.

Figure 5. - Concluded. Turbulent shear stress spectrum.

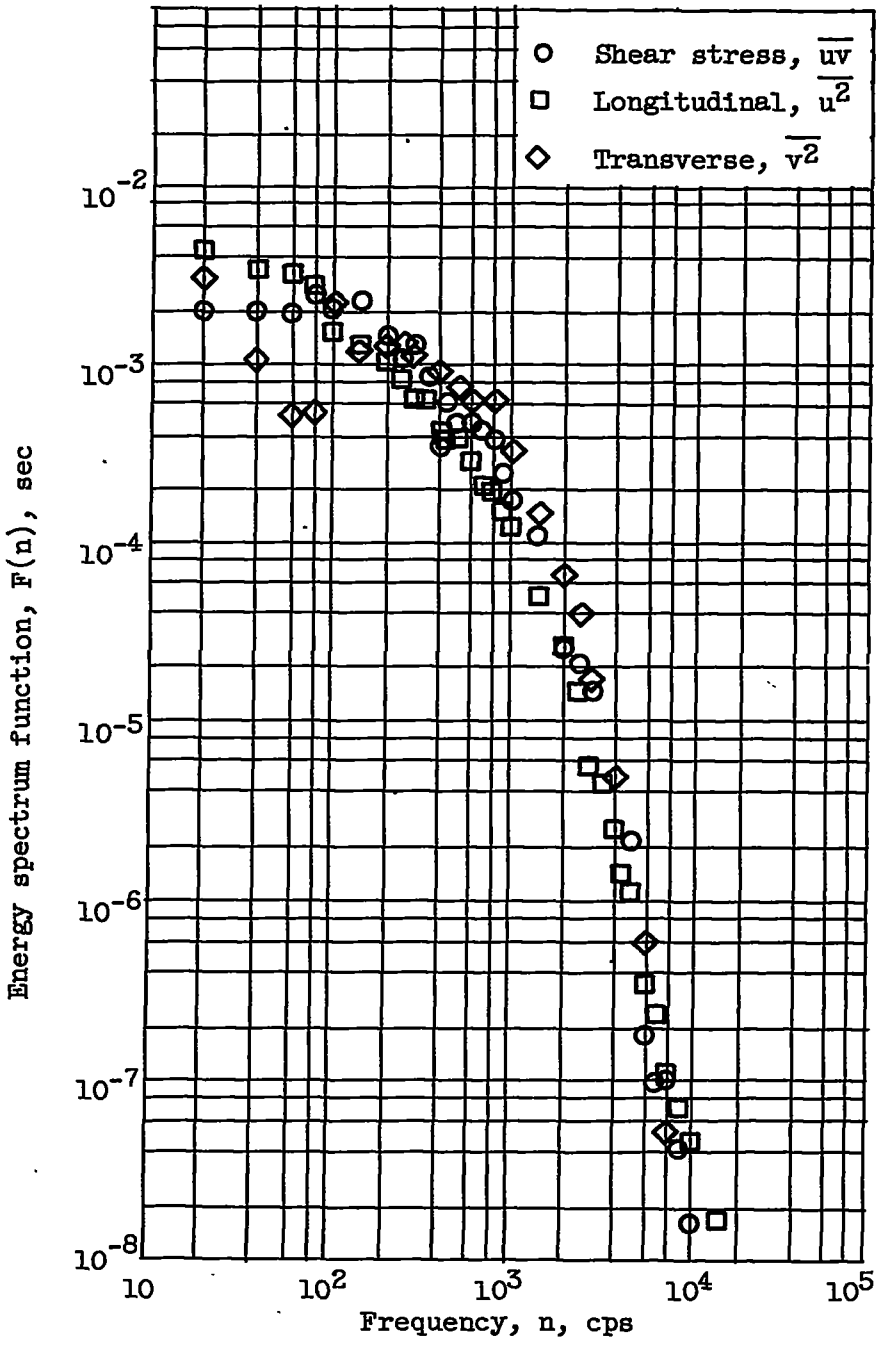

Figure 6. - Comparison of spectra of Reynolds stresses. Station 1; distance from wall, 0.025 inch.

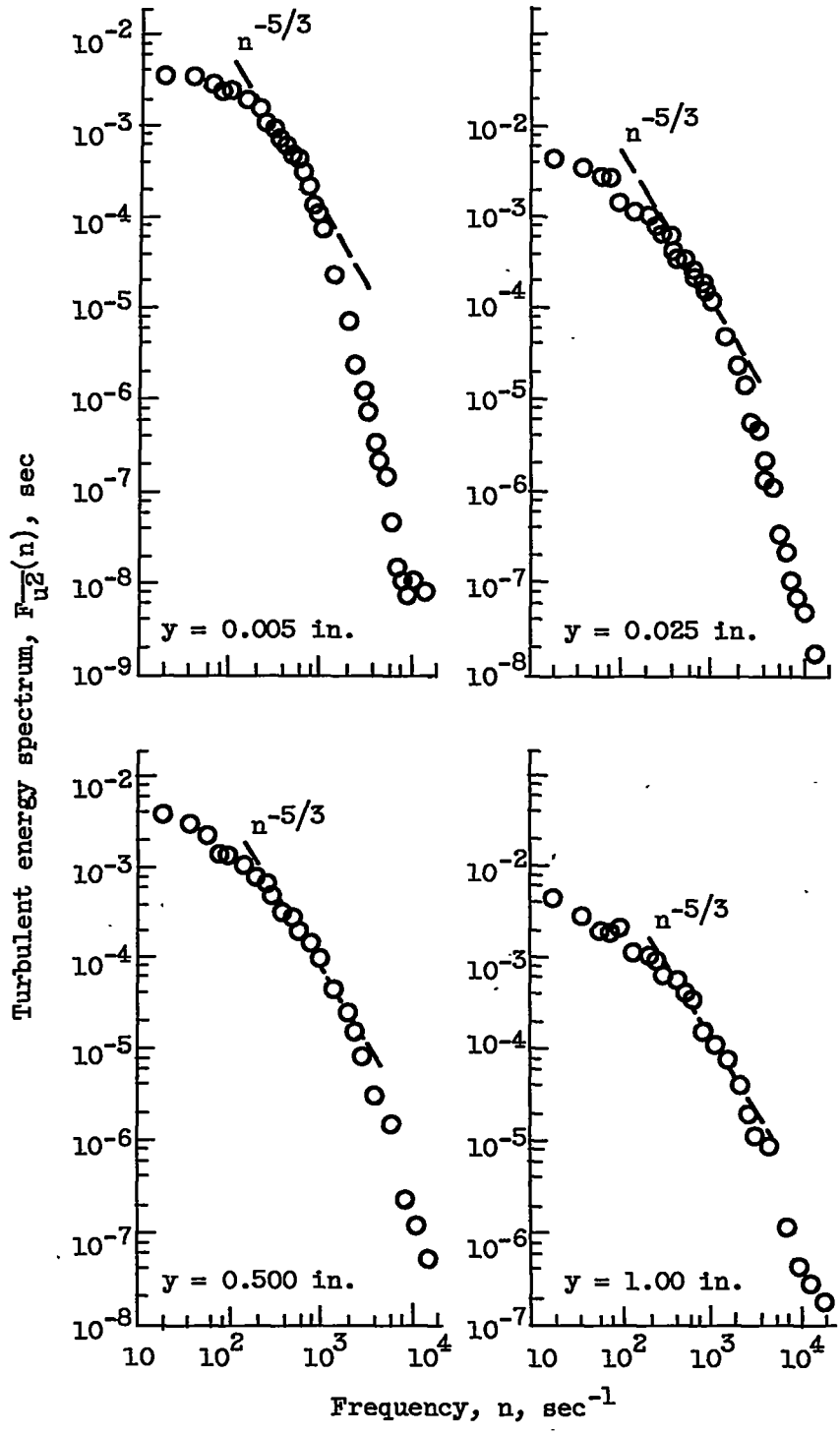

(a) Station 1.

Figure 7. - Longitudinal turbulent velocity spectrum measurements compared with theoretical predictions.

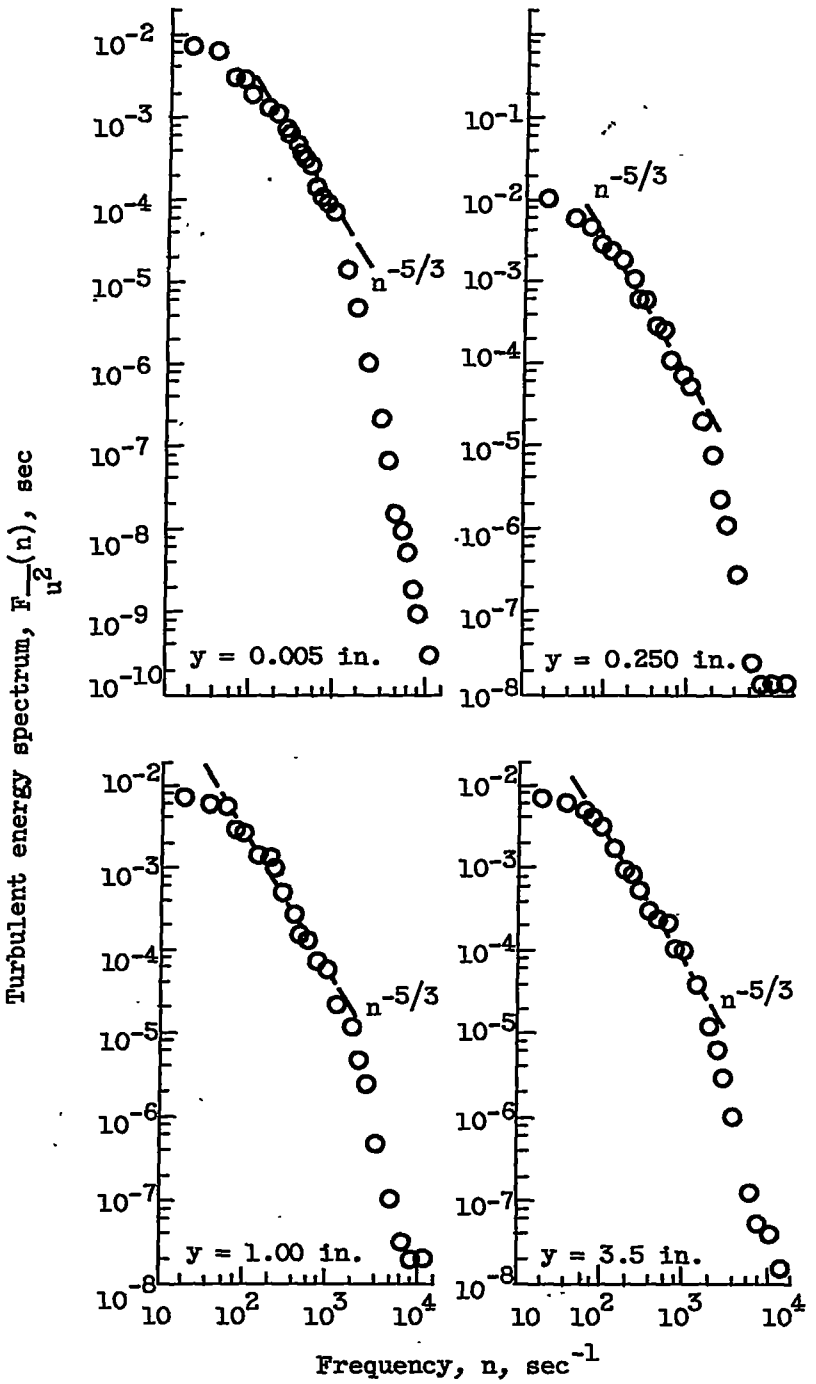

(b) Station 4.

Figure 7. - Concluded. Longitudinal turbulent velocity spectrum measurements compared with theoretical predictions.

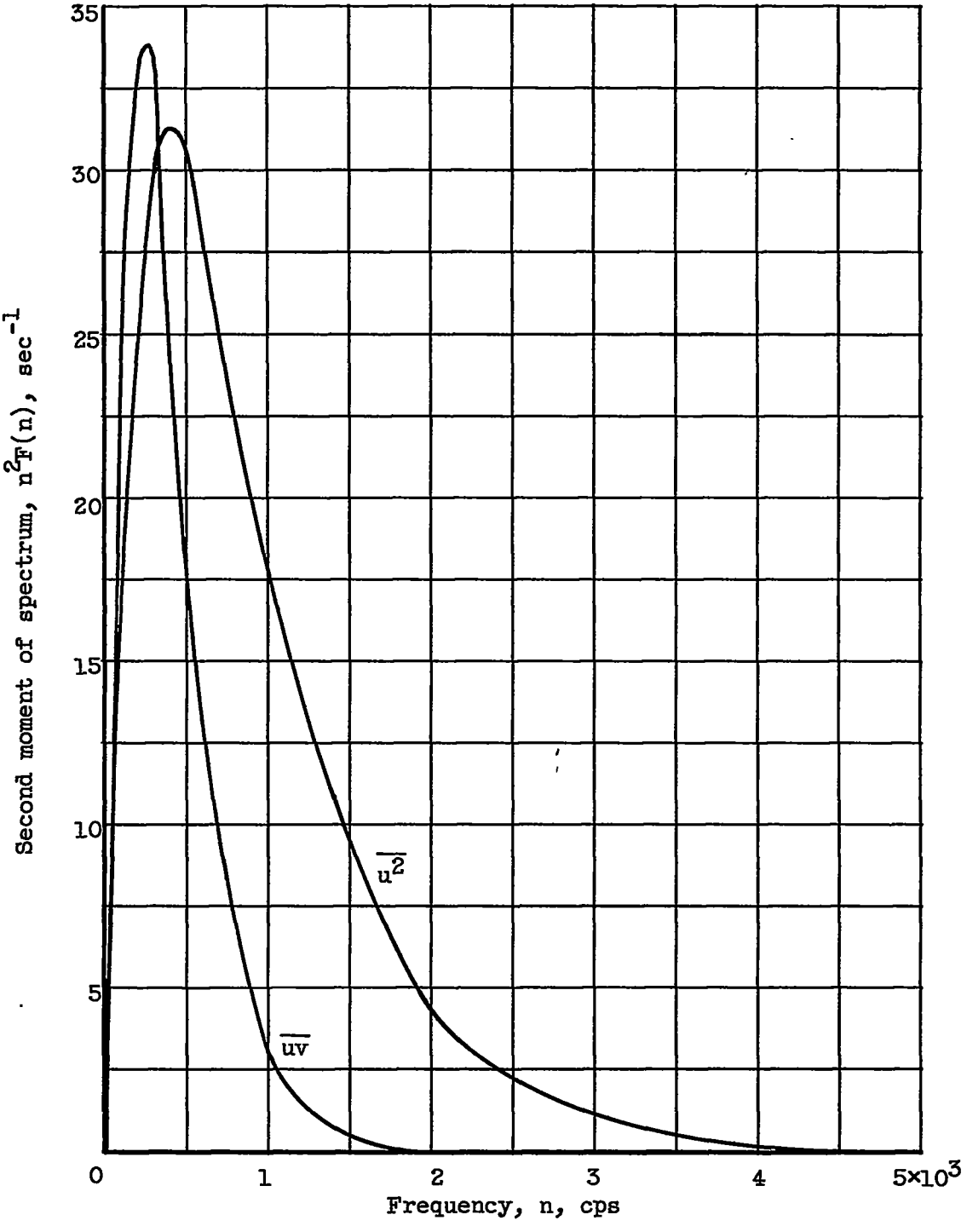

Figure 8. - Comparison of second moments of $F_{\overline{u^2}}(n)$ and $F_{\overline{uv}}(n)$ spectra at a ratio of distance from wall to channel half width of 0.4 for a fully developed turbulent flow between parallel planes (ref. 6).

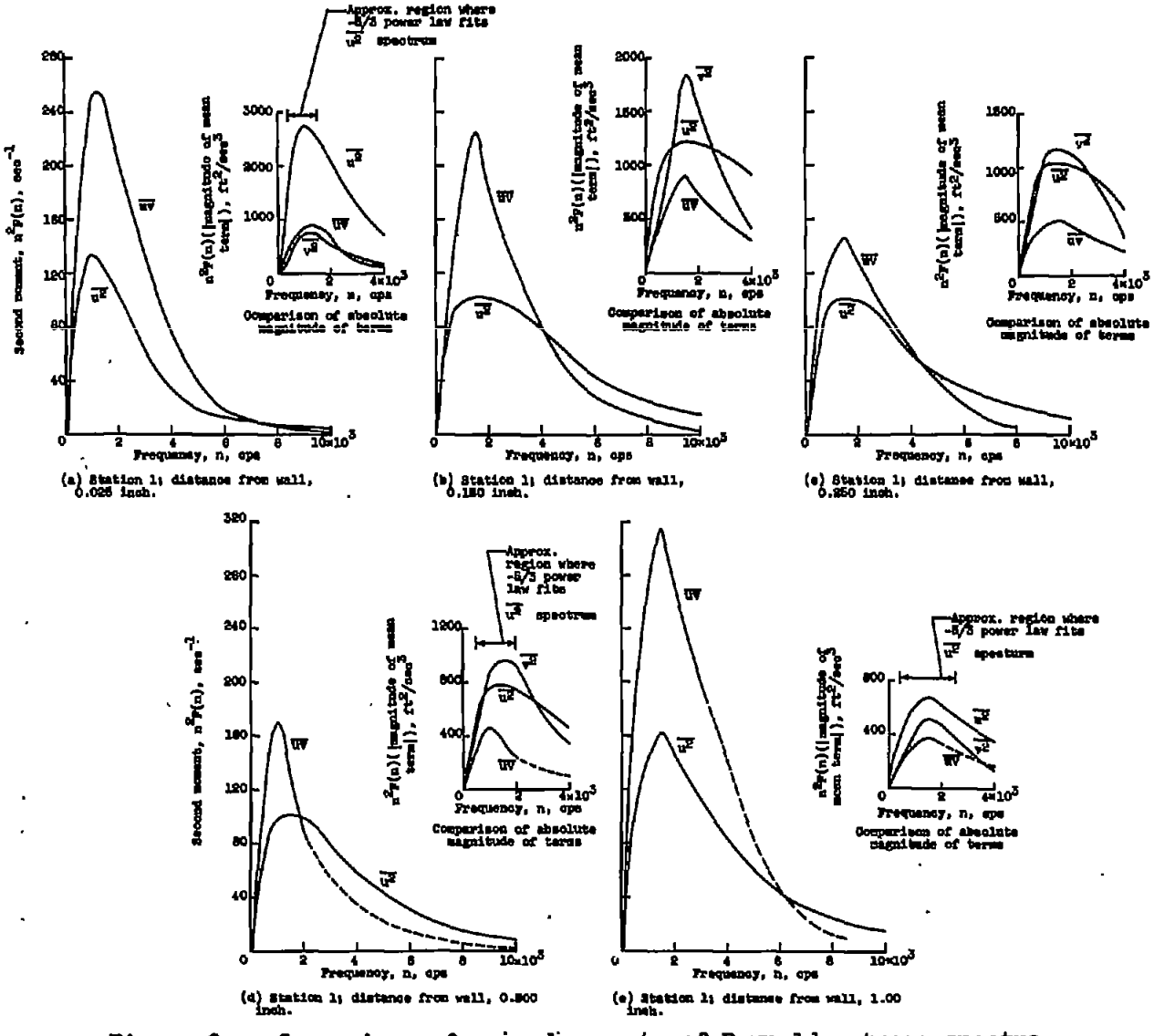

Figure 9. - Comparison of second moments of Reynolds stress spectra.

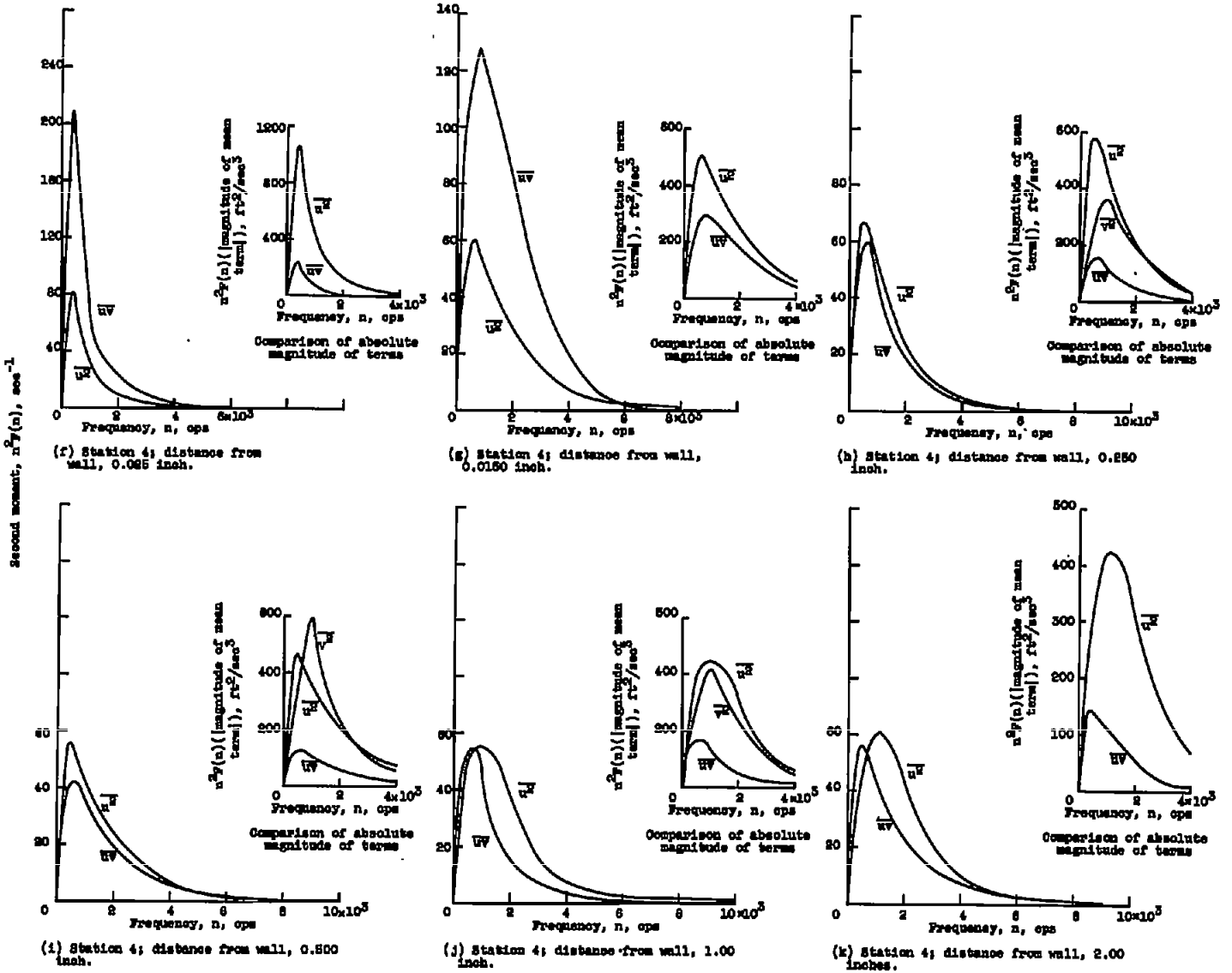

Figure 9. - Continued. Comparison of second moments of Reynolds stress spectra.

(l) Station 4; distance from wall, 3.00 inches.

(m) Station 4; distance from wall, 3.50 inches.

Figure 9. - Concluded. Comparison of second moments of Reynolds stress spectra.

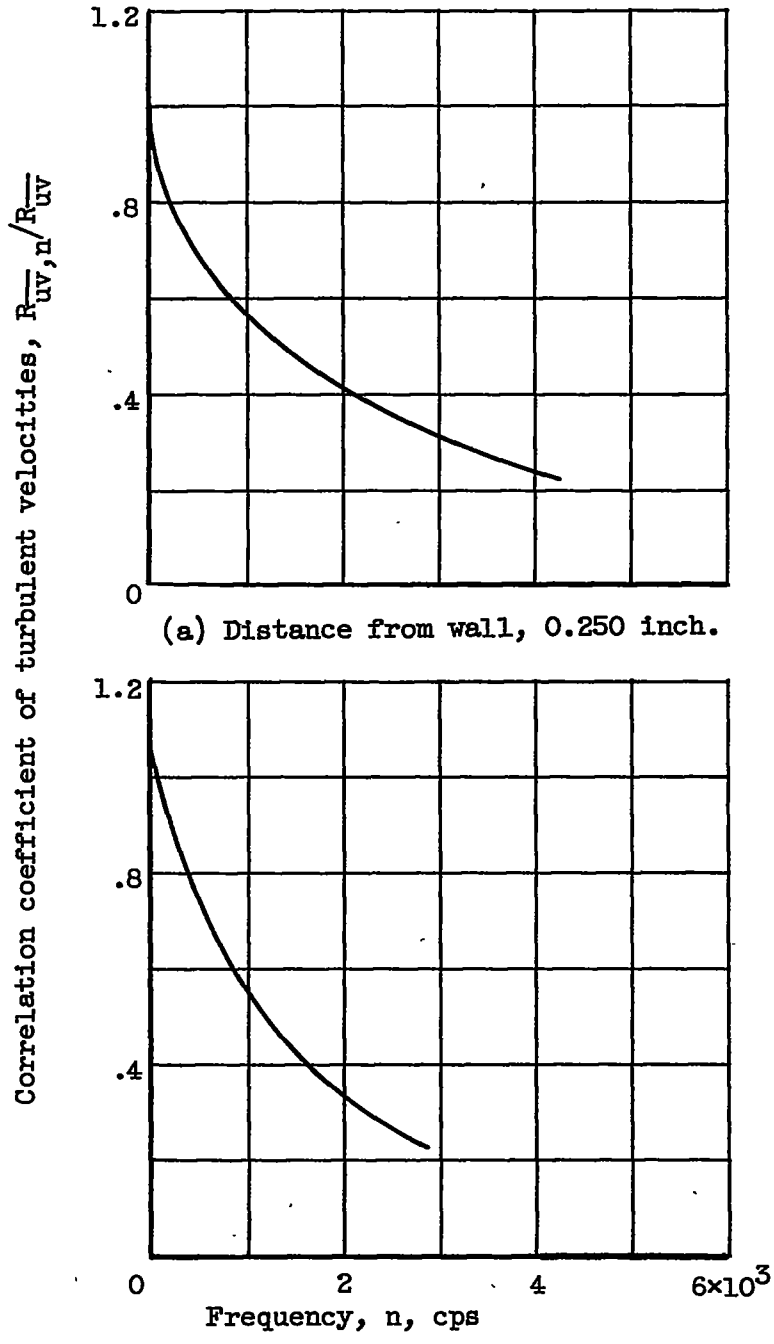

(a) Distance from wall, 0.250 inch.

(b) Distance from wall, 1.00 inch.

Figure 10. - Variation of shear correlation coefficient with frequency. Station 4.

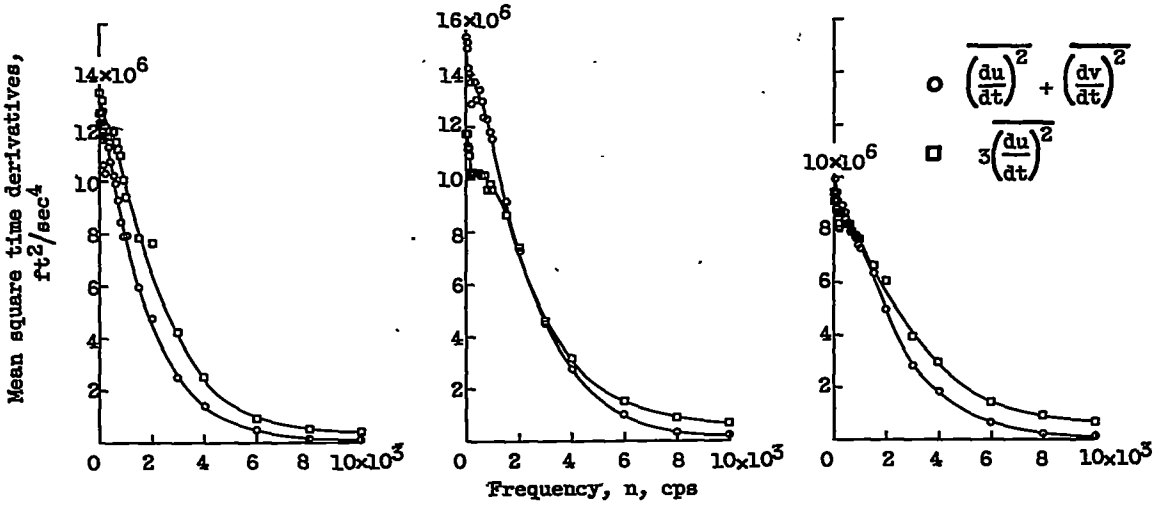

(a) Station 1; distance from wall, 0.025 inch.

(b) Station 1; distance from wall, 0.150 inch.

(c) Station 1; distance from wall, 0.250 inch.

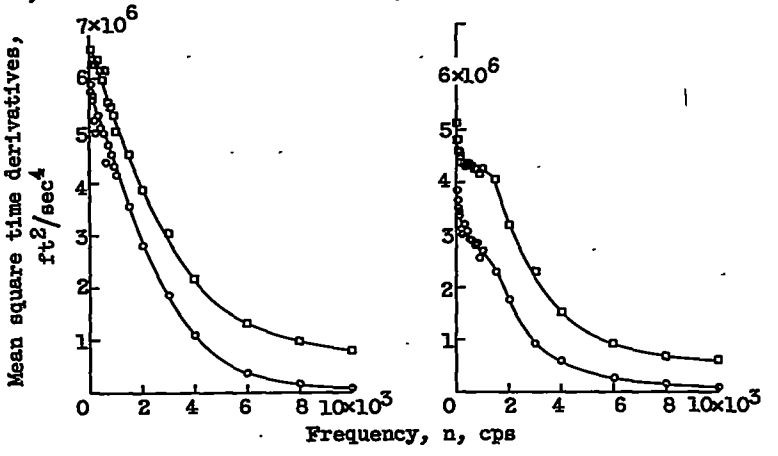

(d) Station 1; distance from wall, 0.500 inch.

(e) Station 1; distance from wall, 1.00 inch.

Figure 11. - Variation of turbulent velocity derivatives with frequency.

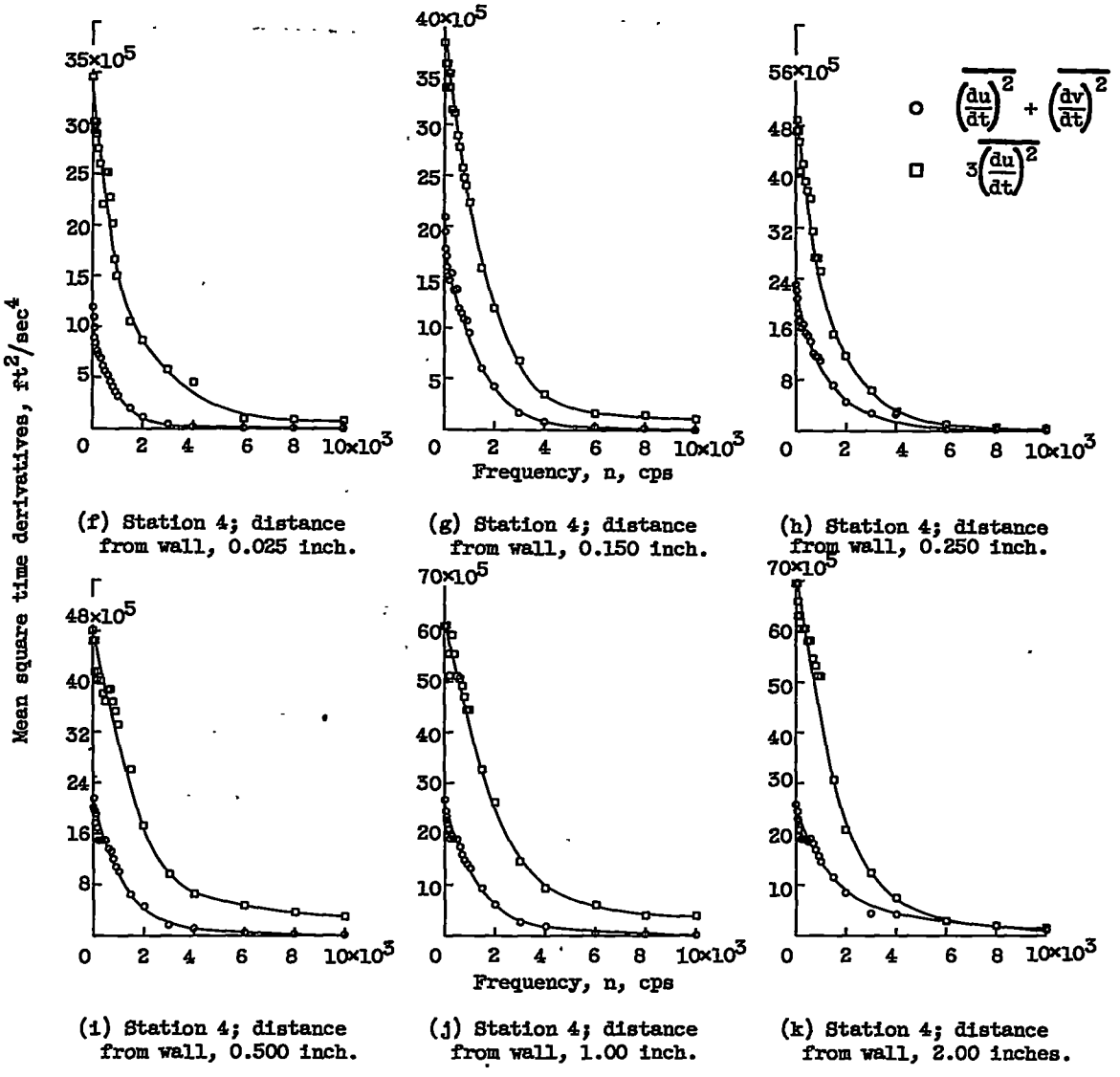

(f) Station 4; distance from wall, 0.025 inch.

(g) Station 4; distance from wall, 0.150 inch.

(h) Station 4; distance from wall, 0.250 inch.

(i) Station 4; distance from wall, 0.500 inch.

(j) Station 4; distance from wall, 1.00 inch.

(k) Station 4; distance from wall, 2.00 inches.

Figure 11. - Continued. Variation of turbulent velocity derivatives with frequency.

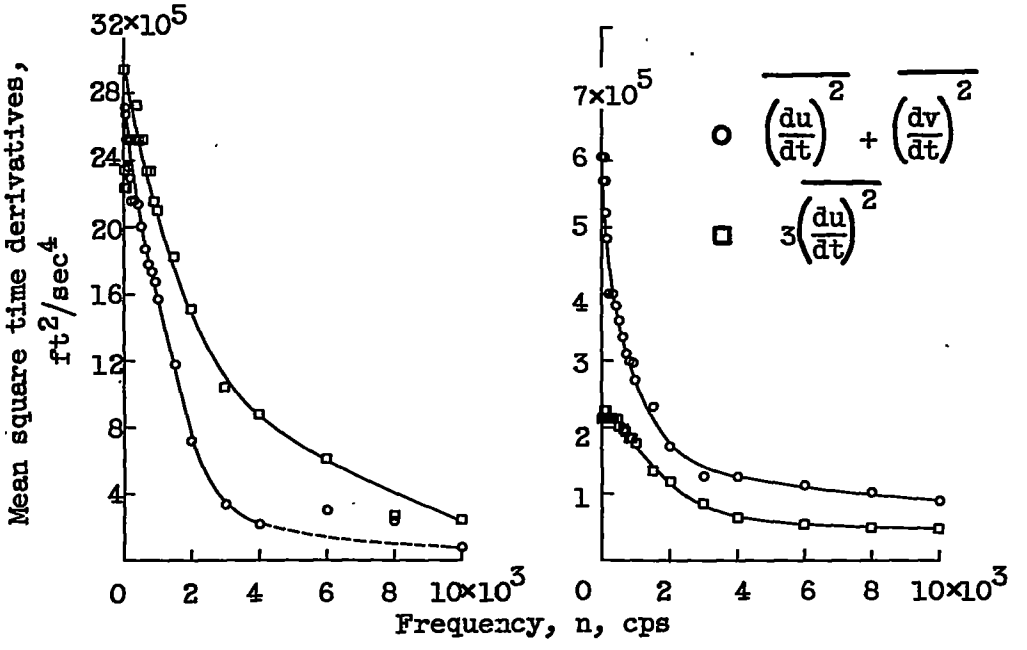

(l) Station 4; distance from wall, 3.00 inches.

(m) Station 4; distance from wall, 4.00 inches.

Figure 11. Concluded. Variation of turbulent velocity derivatives with frequency.

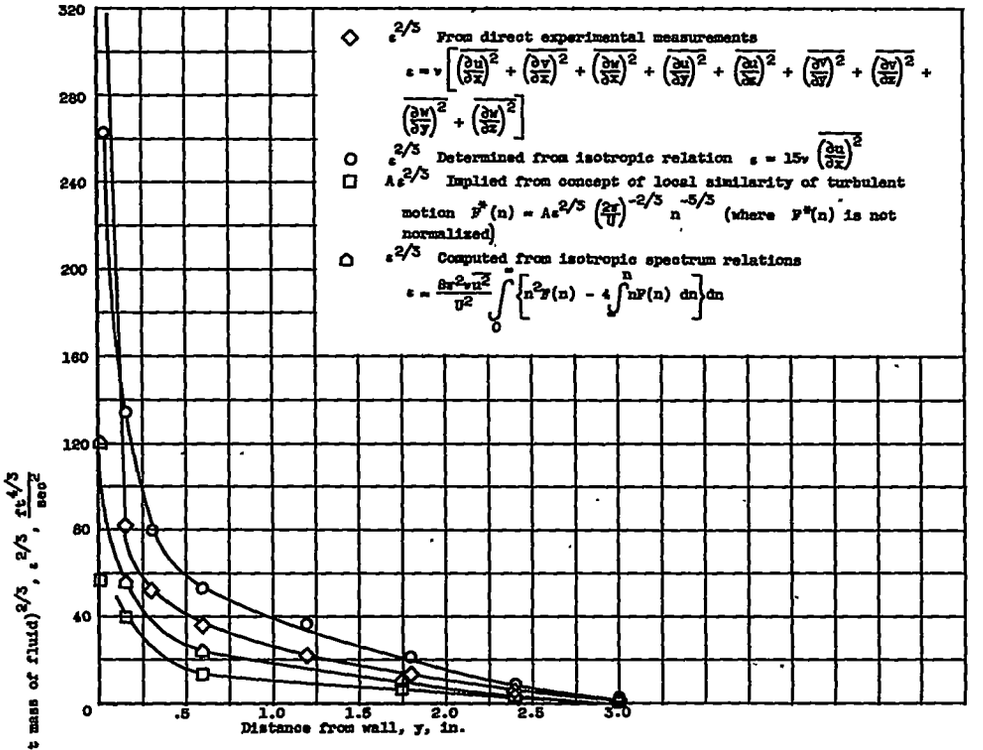

Figure 12. - Comparison of direct and isotropic relations for predicting turbulent energy dissipation (ref. 9.).

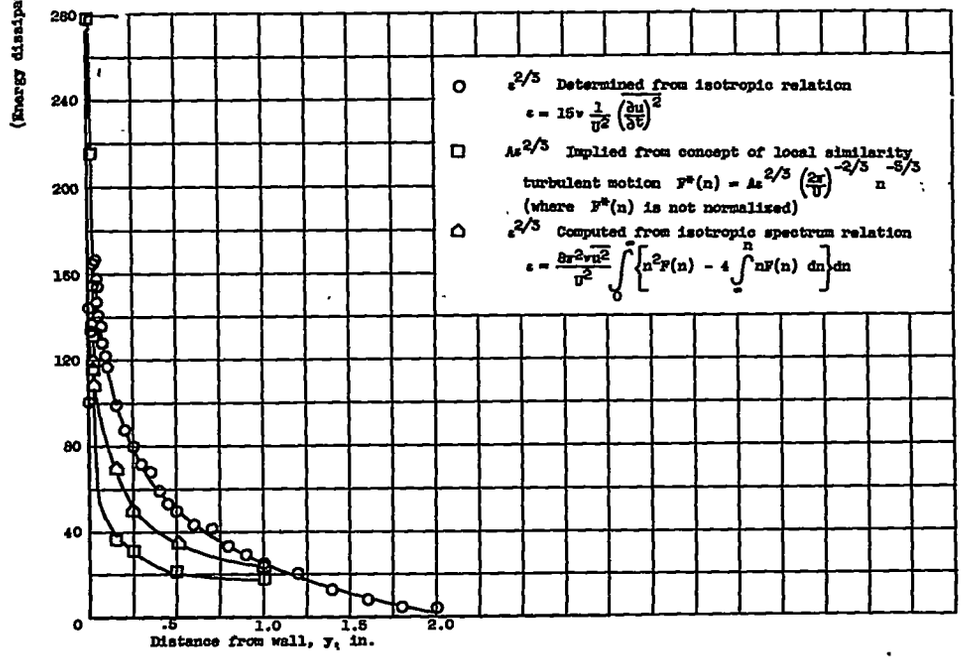

Figure 13. - Variation through boundary layer of turbulent energy dissipation as predicted by isotropic relations. Station 1.

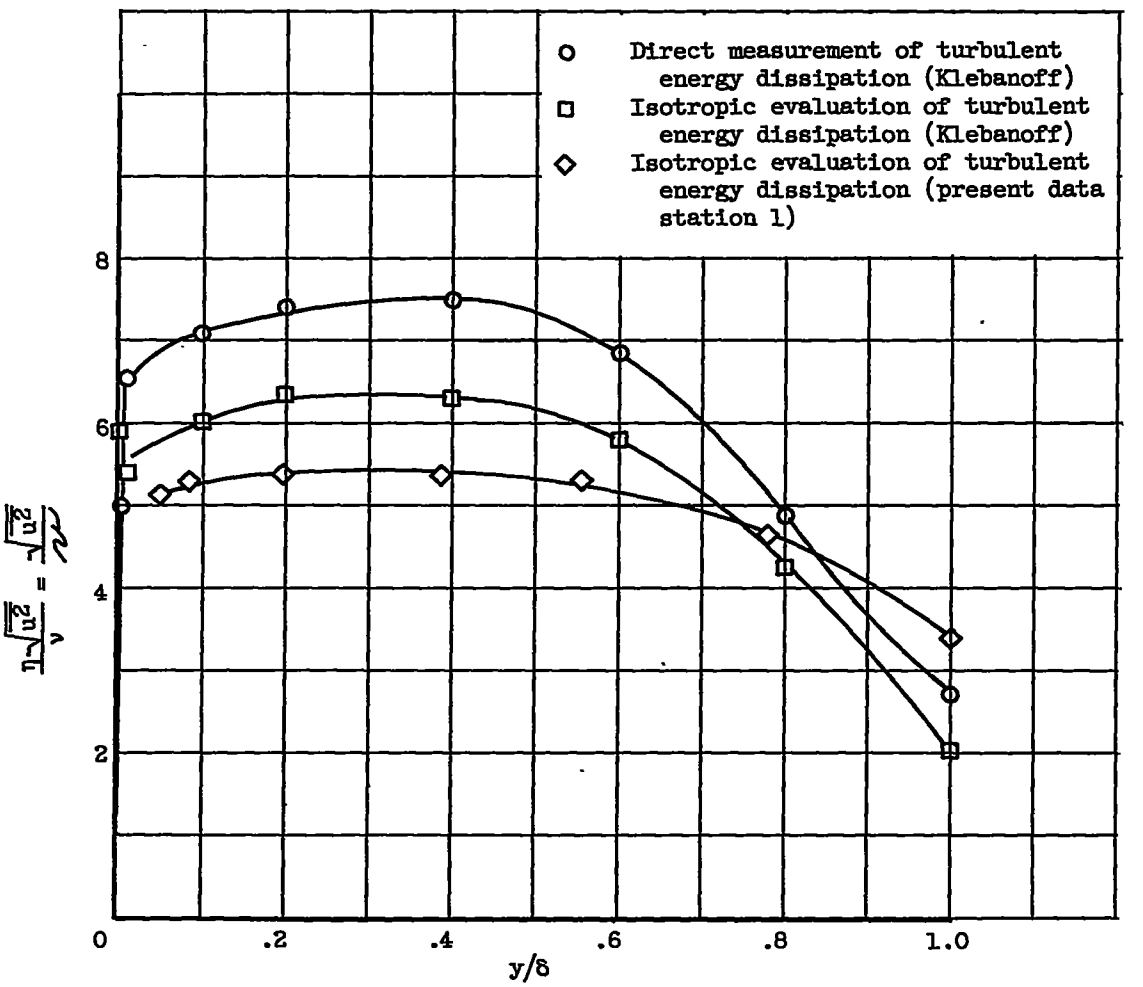

Figure 14. - Universal equilibrium parameters.